Exact PDL-induced SNR statistics in dual-polarization coherent optical communication systems

Research Article Vol. 34, No. 11 / 1 Jun 2026 / Optics Express 19588
Optics EXPRESS

# Exact PDL-induced SNR statistics in dual-polarization coherent optical communication systems

ENRICO MIOTTO,[1,*] ANDREA D'AMICO,[2] STEFANO STRAULLU,[3] TORU MANO,[4] HIDEKI NISHIZAWA,[4] AND VITTORIO CURRI[1]

[1]Department of Electronics and Telecommunications, Politecnico di Torino, 24 Corso Duca degli Abruzzi, Torino 10129, Italy
[2]NEC Laboratories America, 4 Independence Way, Princeton, New Jersey 08540, USA
[3]LINKS Foundation, 61 Via Pier Carlo Boggio, Torino 10138, Italy
[4]NTT Network Innovation Laboratories, 1-1 Hikarinooka, Yokosuka, Kanagawa 239-0847, Japan
[*]enrico.miotto@polito.it

**Abstract:** We derive the exact probability density function of the signal to noise ratio (SNR) impairment caused by polarization dependent loss (PDL) in coherent optical systems. Using the hinge model for PDL statistics, we construct a sequence of variable transformations that yields the expression of the SNR probability density function by means of a sequence of nested recursive integrals. Monte Carlo simulations validate the analytical formulation assuming realistic PDL levels and link configurations, showing excellent agreement. The model accurately captures SNR variability introduced by cascaded PDL elements and provides a foundation for statistical margin assessment, digital twin modeling, and quality of transmission estimation in flexible, low margin optical networks.



## 1. Introduction

The exponential growth of global data traffic, driven by the proliferation of cloud services, hyperscale data centers, and bandwidth intensive applications, continues to challenge the capacity and adaptability of optical transport networks [1,2]. Conventional fixed grid wavelength division multiplexing (WDM) systems have reached their operational limits in terms of spectral efficiency and flexibility, motivating the transition toward flexible optical networks (FONs) [3–5]. By exploiting flex grid spectral allocation and programmable transceivers, FONs can dynamically adjust transmission parameters, such as modulation format, baud rate, and channel bandwidth, to match instantaneous traffic demand and physical layer conditions [6,7]. This architectural evolution enables capacity on demand operation, supporting the broader Network as a Service (NaaS) paradigm in which network resources are virtualized, provisioned dynamically, and managed with guaranteed performance levels [8–10].

Achieving such dynamic adaptability requires accurate physical layer performance estimation, since flex rate transceivers provide substantial gains in overall network throughput, especially when accurate channel knowledge enables operation with reduced performance margins [11]. Network margins are required to guarantee error free operation over the system's lifetime, whether during new network roll out or the upgrade of existing infrastructure. Nevertheless, such margins incur a cost in the form of over dimensioning, and should thus be kept as small as possible [12,13]. To address this challenge, optical network digital twins (ONDTs) are emerging as a powerful tool to enhance network observability and predictive performance assessment [14]. An ONDT, which is a virtual replica continuously synchronized with real network telemetry, can integrate analytical models, data driven estimators, and operational measurements to provide accurate and up to

#587873 https://doi.org/10.1364/OE.587873
Journal © 2026 Received 15 Dec 2025; revised 4 Apr 2026; accepted 24 Apr 2026; published 19 May 2026

Optics EXPRESS

date representations of physical layer conditions [15]. By enabling what-if analyses, predictive maintenance, and closed loop optimization, ONDTs facilitate dynamic margin adaptation and proactive impairment mitigation, thus reducing the dependency on static design margins and improving overall network efficiency [16,17].

When estimating performance, the focus should be in particular on the signal-to-noise ratio (SNR), which directly determines the achievable bit rate and modulation format selection. Flexible transceivers rely on precise channel state information to optimize spectral efficiency while maintaining a target quality of transmission (QoT). Inaccurate SNR estimation can lead to either overestimation, resulting in degraded performance, or underestimation, leading to inefficient use of spectral resources. Therefore, the development of analytical models capable of capturing the statistical behavior of the SNR under realistic impairment conditions is crucial for both real time network operation and long-term planning.

Among the various physical impairments affecting coherent optical systems, polarization dependent loss (PDL) remains one of the most difficult to model accurately. PDL can arise due to several optical components; including connectors, multiplexers, and amplifiers [18–20]; but the most significant amount of PDL is introduced by Wavelength Selective Switches (WSSs) in Reconfigurable Add-Drop Optical Multiplexer (ROADMs) [21]. The PDL effect consists of unequal attenuation on orthogonal polarization states of the signal crossing the device, which depends on the state of polarization of the incoming signal. Although typically small in magnitude, it has a random and time-varying nature caused by random polarization rotations in optical fibers due to birefringence, mechanical stress, and temperature fluctuations [22,23]. In addition, the PDL introduced by ROADMs is also dependent on port and frequency [24–26]. PDL is responsible for fluctuations in the received optical power and interacts with amplified spontaneous emission (ASE) noise [27] and polarization mode dispersion (PMD) [28]. In coherent detection systems employing polarization multiplexing, these effects translate into stochastic variations of the SNR [29], which can compromise the reliability of adaptive transmission schemes and margin based resource allocation algorithms. The current paradigm is to establish a worst-case margin based on the PDL accumulation along the optical link [30]. Nevertheless, such an approach turns out to be highly inefficient and too conservative due to the low probability of extreme PDL events. Knowing the probability density function (PDF) of the PDL-induced SNR it is possible to assess a statistical margin based on the desired probability of out of service (POOS) [26,31,32].

Many mitigation techniques have been proposed to reduce QoT fluctuation in the presence of PDL [33–35], and the PDL statistic has been widely investigated analytically, experimentally, and through numerical simulations [36–39]. Nevertheless, a comprehensive analytical treatment of its effect on SNR remains limited. Analytical modeling offers several advantages: it enables closed form statistical characterization, facilitates insight into the physical mechanisms underlying SNR fluctuations, and supports fast, scalable QoT estimation required by real-time control and optimization in elastic optical networks. In addition, analytical frameworks provide the mathematical foundation for margin prediction and impairment aware resource allocation, and they can also complement data driven methods in scenarios such as machine-learning-assisted network automation. A first step on analytical modeling of PDL-induced SNR was performed in [40], where the derivation of the statistic of the SNR degradation in presence of PDL is performed for intensity modulated optical systems. Moreover, in [40] a continuous model is assumed to describe the distribution of the PDL along the optical link, which is accurate only in long systems with a large number of PDL elements. In [31], the performance degradation in coherent polarization multiplexed systems was analyzed under the assumptions of low PDL and negligible nonlinear interference (NLI), introducing a statistical margin approach based on a discretized PDL distribution along the optical link. In [29] the "hinge model" for PDL was proposed, following the approach previously adopted for PMD [41], and using the PDF derived in [42] for PMD and adapted to PDL as an approximation, focusing on the PDL distribution rather

Optics EXPRESS

than on its impact on the SNR. In [43] a statistical characterization of the PDL impact on OSNR is provided, based on Monte Carlo simulation, and a disaggregated Gaussian approximation of the PDF of the SNR is proposed. Regarding the interaction between PDL and Kerr nonlinearity in the generation of nonlinear interference (NLI) noise under the additive Gaussian approximation for dual-polarization coherent systems [44,45], several studies have provided important insights. In [46,47], it was shown that PDL affects the amount of generated NLI primarily in dispersion-managed (DM) links, whereas in the widely deployed dispersion-uncompensated transmission systems, the NLI level is only marginally influenced by PDL. An extension of the GN-model [44] accounting for PDL in NLI accumulation was proposed in [48]; however, its use relies on a Monte Carlo framework, which leaves a gap with respect to a fully analytical description. Motivated by these considerations, in this work we develop an analytical model for the impact of PDL on the SNR in dispersion-uncompensated coherent optical transmission systems, assuming ASE noise only and ideal equalization at the receiver. The NLI contribution can be incorporated into the proposed framework using the Gaussian-channel model of [32], in which NLI is treated as a worst-case Gaussian noise source at the receiver.

The main contribution of this work is, to the best of our knowledge, the first analytical derivation of the probability density function (PDF) of the PDL-induced SNR. We build on the statistics of the attenuation caused by PDL, described by the hinge model in [38], which provides the foundation of the present analysis. In dual-polarization coherent systems, PDL affects the two recovered tributaries in a correlated manner. In this paper, however, we focus on the exact marginal PDF of the SNR on a single polarization axis; by symmetry, the same marginal distribution applies to the other tributary as well. Although the joint dual-polarization SNR distribution is beyond the scope of the present work, the derived marginal PDF is still of practical relevance, since it enables the statistical characterization of either tributary individually. This is particularly useful in practical implementations, where monitoring is often available on a per-tributary basis, thereby supporting telemetry-driven margin estimation. The proposed framework should be interpreted within its modeling scope. In particular, it isolates the contribution of frequency-flat PDL to SNR fluctuations in the presence of additive ASE noise and ideal equalization. Chromatic dispersion is not included because, being a linear lossless impairment, it does not affect the present derivation under the assumption of ideal equalization. By contrast, PMD, filtering-induced distortions, and practical equalizer implementation penalties may interact with PDL in a non-trivial way and are therefore outside the scope of the present work. The rigorous derivation is presented in Section 2, where the key step consists in introducing a variable transformation that simplifies the Jacobian determinant and makes the analytical formulation of the PDL-induced SNR PDF tractable. The validation through Monte Carlo simulation is provided in Section 3, for an increasing number of devices and PDL magnitude, with some insights on the obtained PDF functions. The derived expression bridges the gap between component-level polarization effects and system-level performance estimation, enabling improved accuracy in QoT prediction and adaptive margin assessment. These results contribute to the analytical foundation necessary for the realization of truly elastic, capacity-on-demand optical networks capable of supporting the evolving requirements of data-intensive communication infrastructures.

## 2. Mathematical derivation of the probability density function of the PDL-induced SNR

The reference system for the derivation of the PDL-induced SNR PDF is provided in Fig. 1. We perform the derivation considering the SNR on the X polarization; therefore, the power of the noise sources and the power of the signal are half of the total power of the coherent dual-polarization scenario. For the Y polarization, the derivation of the PDF of the PDL-induced SNR follows the same procedure. Indeed, the PDL-induced SNR distribution is expected to be the same in both X and Y polarizations, which was confirmed through simulations and experiments

Optics EXPRESS

in [26,27]. The link is composed of a cascade of $N$ PDL devices, which could be ROADMs, attenuating the signal and the additive noise. The PDL devices are alternated with noise sources, of power $p_{n,1}, \ldots, p_{n,N+1}$, which can be injected along the link due to optical amplification. As stated above, we consider the NLI effect, if not negligible, as embedded in the final noise source $p_{n,N+1}$ [32]. At the end of the link, the DSP block is assumed to perform an ideal equalization, inverting the attenuation experienced by the transmitted signal. The transmitted power on the X polarization is represented by $p_s$.

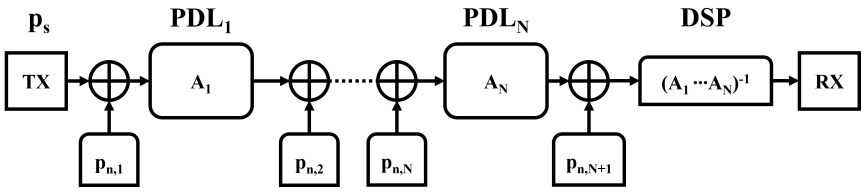


**Fig. 1.** Mathematical abstraction of PDL-impaired optical link, with definition of indexes.

The attenuation caused by each PDL device on the X polarization, neglecting the polarization independent loss and considering the randomization of polarization of the signal impinging upon each PDL element due to birefringence, is uniformly distributed according to [38], where the derivation of such a model is based on Jones Calculus [49]. The PDFs of the N attenuations introduced by all the PDL devices are expressed as:

$$f_{A_i}(x) = \frac{\sqrt{1-\gamma_i^2}}{2\gamma_i}; \quad x \in \left[\xi_i^{-1} \triangleq \frac{\sqrt{1-\gamma_i}}{\sqrt{1+\gamma_i}}; \xi_i \triangleq \frac{\sqrt{1+\gamma_i}}{\sqrt{1-\gamma_i}}\right]; \quad i = 1, \ldots, N; \tag{1}$$

where each term $\gamma_i$ $(i = 1, \ldots, N)$ can be obtained from the characterization of the i-th PDL device which provides the parameter $PDL_{dB,i}$. $PDL_{dB,i}$ represents the power ratio, expressed in decibels, between the least and the most attenuated states of polarization entering the device.

$$\gamma_i = \frac{10^{\frac{PDL_{dB,i}}{10}} - 1}{10^{\frac{PDL_{dB,i}}{10}} + 1} \in [0, 1]; \quad i = 1, \ldots, N. \tag{2}$$

The attenuations $A_i$ are independent uniform-distributed random variables. We compute the SNR at the end of the line on the X polarization, assuming ideal equalization.

$$\begin{aligned} \mathrm{SNR} &= \frac{p_s \prod_{i=1}^{N} A_i \cdot \prod_{l=1}^{N} A_l^{-1}}{\sum_{j=1}^{N+1} p_{n,j} \prod_{k=j}^{N} A_k \cdot \prod_{l=1}^{N} A_l^{-1}} \\ &= \frac{p_s}{\sum_{j=1}^{N+1} p_{n,j} \prod_{k=1}^{j-1} A_k^{-1}}. \end{aligned} \tag{3}$$

To simplify the analysis we compute the $\mathrm{SNR}^{-1}$, which is expressed as a sum of $N + 1$ terms:

$$\mathrm{SNR}^{-1} = \frac{1}{p_s}\left(p_{n,1} + \sum_{i=1}^{N} \frac{p_{n,i+1}}{\prod_{j=1}^{i} A_j}\right); \tag{4}$$

we define the random variables $X_i$ as the reciprocal of the random variables $A_i$:

$$X_i = \frac{1}{A_i}; \quad i = 1, \ldots, N. \tag{5}$$

Optics EXPRESS

The corresponding PDFs are obtained through the well-known formula for the inverse of a random variable:

$$f_{X_i}(x_i) = \frac{1}{x_i^2} \cdot \frac{\sqrt{1-\gamma_i^2}}{2\gamma_i}; \quad i = 1, \ldots, N. \tag{6}$$

All $X_i$ are independent, and their supports are the same as $A_i$, namely: $[\xi_i^{-1}; \xi_i]$ for $i = 1, \ldots, N$. Now we can express the $\mathrm{SNR}^{-1}$ in a simpler way:

$$\mathrm{SNR}^{-1} = \frac{1}{p_s}\left(p_{n,1} + \sum_{i=1}^{N} p_{n,i+1} \prod_{j=1}^{i} X_j\right). \tag{7}$$

To obtain the PDF expression, we proceed in three steps. First, we focus on $\mathrm{SNR}^{-1}$ and compute its cumulative distribution function (CDF); then we evaluate the derivative of the CDF to obtain the PDF; finally, we apply the inversion formula to get the PDF of the SNR.

The CDF of $\mathrm{SNR}^{-1}$ is obtained by integrating the joint PDF of the N random variables $X_i$.

$$F_{\mathrm{SNR}^{-1}}(z) = Prob\{\mathrm{SNR}^{-1} \leq z\} = \int\int\cdots\int_{\chi:\mathrm{SNR}^{-1}\leq z} dx_1 \ldots dx_N \cdot f_{X_1,\ldots,X_N}(x_1, \ldots, x_N); \tag{8}$$

where the joint PDF is the product of the single PDFs due to variable independence:

$$f_{X_1,\ldots,X_N}(x_1, \ldots, x_N) = \prod_{i=1}^{N} \frac{1}{x_i^2} \frac{\sqrt{1-\gamma_i^2}}{2\gamma_i}. \tag{9}$$

By substituting Eq. (9) in Eq. (8) we obtain:

$$F_{\mathrm{SNR}^{-1}}(z) = \eta \cdot \int\int\cdots\int_{\chi:\mathrm{SNR}^{-1}\leq z} dx_1 \ldots dx_N \prod_{i=1}^{N} \frac{1}{x_i^2}; \tag{10}$$

where $\eta = \prod_{i=1}^{N} \frac{\sqrt{1-\gamma_i^2}}{2\gamma_i}$ for compact notation. The integrand function is quite simple, but the integration domain depends on a complex nonlinear multi-dimensional condition, which involves all the random variables $X_i$. We proceed by applying an opportune change of variable. We choose the following set of functions:

$$Y_k = p_{n,k} + X_k \cdot \left(p_{n,k+1} + \sum_{i=k+1}^{N} p_{n,i+1} \prod_{j=k+1}^{i} X_j\right). \tag{11}$$

We point out that such change of variables does not apply only to the case of uniform random variables, which is the focus of this work on PDL. It is useful in general when dealing with problems in which the statistical evaluation of SNR depends on the interplay of cascaded elements and noise sources, following the structure of the link in Fig. 1. Equation (11) allows an equivalent recursive expression:

$$\begin{cases} X_k = \frac{Y_k - p_{n,k}}{Y_{k+1}} & k = 1, \ldots, N-1 \\ X_N = \frac{Y_N - p_{n,N}}{p_{n,N+1}} \end{cases} \tag{12}$$

Subject to the following support conditions, which impact the nested integration boundaries:

$$\begin{cases} \xi_k^{-1} \leq \frac{Y_k - p_{n,k}}{Y_{k+1}} \leq \xi_k & k = 1, \ldots, N-1 \\ \xi_N^{-1} \leq \frac{Y_N - p_{n,N}}{p_{n,N+1}} \leq \xi_N \end{cases} \tag{13}$$

Optics EXPRESS

The Jacobian of the transformation is upper-triangular:

$$J = \begin{pmatrix} \frac{1}{Y_2} & -\frac{Y_1 - p_{n,1}}{Y_2^2} & 0 & 0 & \dots & \dots & \dots & 0 \\ 0 & \frac{1}{Y_3} & -\frac{Y_2 - p_{n,2}}{Y_3^2} & 0 & \dots & \dots & \dots & 0 \\ \vdots & \ddots & \ddots & \ddots & \ddots & & & \vdots \\ 0 & \dots & 0 & \frac{1}{Y_k} & -\frac{Y_{k-1} - p_{n,k-1}}{Y_k^2} & 0 & \dots & 0 \\ \vdots & & & \ddots & \ddots & \ddots & \ddots & \vdots \\ \vdots & & & & \ddots & \ddots & \ddots & 0 \\ 0 & \dots & \dots & \dots & \dots & 0 & \frac{1}{Y_N} & -\frac{Y_{N-1} - p_{n,N-1}}{Y_N^2} \\ 0 & \dots & \dots & \dots & \dots & \dots & 0 & \frac{1}{p_{n,N+1}} \end{pmatrix} \tag{14}$$

To perform the change of variable in resolving the integral of Eq. (10) we need the modulus of the determinant of the Jacobian:

$$|det(J)| = \frac{1}{p_{n,N+1}} \cdot \prod_{i=2}^{N} \frac{1}{Y_i}. \tag{15}$$

Substituting (12) and (15) in Eq. (10), we are able to separate the integration domains, obtaining N nested recursive integrals:

$$\begin{aligned} F_{\mathrm{SNR}^{-1}}(z) = \eta \cdot p_{n,N+1} \int_{p_s \cdot \mathrm{SNR}_{min}^{-1}}^{p_S \cdot z} dy_1 \frac{1}{(y_1 - p_{n,1})^2} \int_{f_1(y_1)}^{g_1(y_1)} dy_2 \frac{y_2}{(y_2 - p_{n,2})^2} \cdots \\ \cdots \int_{f_{k-1}(y_{k-1})}^{g_{k-1}(y_{k-1})} dy_k \frac{y_k}{(y_k - p_{n,k})^2} \cdots \int_{f_{N-1}(y_{N-1})}^{g_{N-1}(y_{N-1})} dy_N \frac{y_N}{(y_N - p_{n,N})^2}; \end{aligned} \tag{16}$$

where the variable $z$ spans a finite continuous interval that ranges from $\mathrm{SNR}_{min}^{-1}$ to $\mathrm{SNR}_{max}^{-1}$ that have the following expressions:

$$\begin{aligned} \mathrm{SNR}_{min}^{-1} &= \frac{1}{p_s} \left( p_{n,1} + \sum_{i=1}^{N} \frac{p_{n,i+1}}{\prod_{k=1}^{i} \frac{\sqrt{1+\gamma_k}}{\sqrt{1-\gamma_k}}} \right); \\ \mathrm{SNR}_{max}^{-1} &= \frac{1}{p_s} \left( p_{n,1} + \sum_{i=1}^{N} \frac{p_{n,i+1}}{\prod_{k=1}^{i} \frac{\sqrt{1-\gamma_k}}{\sqrt{1+\gamma_k}}} \right). \end{aligned} \tag{17}$$

The integration domains defined in Eq. (16) by the functions $f_k(y_k)$ and $g_k(y_k)$ for $k = 1, \dots, N-1$ can be obtained through the constraints (13). At each integration level two conditions must be satisfied to delimit the integration variable. First, from the first $N-1$ inequalities of (13), each $y_k$ for $k = 2, \dots, N$ is subjected to:

$$\begin{cases} y_k \le \xi_{k-1}(y_{k-1} - p_{n,k-1}) \\ y_k \ge \xi_{k-1}^{-1}(y_{k-1} - p_{n,k-1}) \end{cases} \qquad k = 2, \dots, N-1. \tag{18}$$

Therefore, each $y_k$ for $k = 2, \dots, N$ is bounded between two slopes depending on the variable $y_{k-1}$, which is the integration variable of the successive external integral. In addition, starting from the last inequality of (13) (when $k = N$), and proceeding recursively, we obtain that each $y_k$

Optics EXPRESS

is bounded also between two constant values, namely $A_k \leq y_k \leq B_k$, that can be computed at each integration level as:

$$A_k = p_{n,k} + \sum_{i=k}^{N} p_{n,i+1} \prod_{j=k}^{i} \xi_j^{-1}; \quad k = 2, \ldots, N; \tag{19}$$

$$B_k = p_{n,k} + \sum_{i=k}^{N} p_{n,i+1} \prod_{j=k}^{i} \xi_j; \quad k = 2, \ldots, N. \tag{20}$$

The integration domain at each integration level $k$ is graphically represented in Fig. 2. The integration variable $y_k$ is reported in the vertical axis and its boundaries depend on the outer variable $y_{k-1}$ on the horizontal axis.

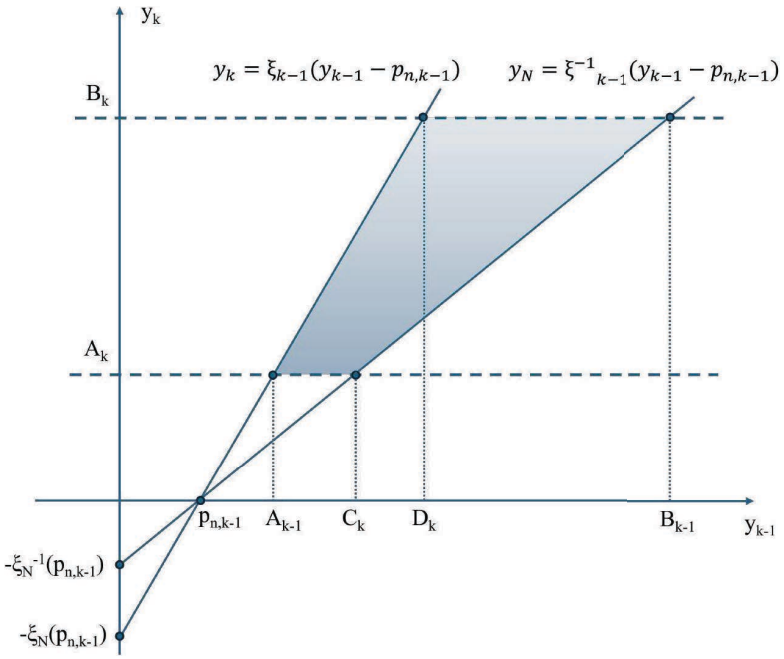


**Fig. 2.** Picture of the integration domain at the $k$-th level of integration.

From Fig. 2 it is possible to understand how to compute the integration limits at each $k$-th integration step, obtaining the functions $f_1(y_1), \ldots, f_{N-1}(y_{N-1})$. Such functions, bounding the $k$-th integration variable $y_k$, are monotone continuous increasing functions of the outer variable $y_{k-1}$, which can be defined piecewise:

$$f_{k-1}(y_{k-1}) = \begin{cases} A_k & y_{k-1} \leq C_k \\ \xi_{k-1}^{-1} \cdot (y_{k-1} - p_{n,k-1}) & y_{k-1} > C_k \end{cases} \quad k = 2, \ldots, N; \tag{21}$$

$$g_{k-1}(y_{k-1}) = \begin{cases} \xi_{k-1} \cdot (y_{k-1} - p_{n,k-1}) & y_{k-1} \leq D_k \\ B_k & y_{k-1} > D_k \end{cases} \quad k = 2, \ldots, N; \tag{22}$$

where $C_k$ and $D_k$ can easily be obtained from $A_k$ and $B_k$:

$$C_k = p_{n,k-1} + \xi_{k-1} A_k; \quad k = 2, \ldots, N; \tag{23}$$

$$D_k = p_{n,k-1} + \xi_{k-1}^{-1} B_k \quad k = 2, \ldots, N. \tag{24}$$

Optics EXPRESS

The CDF is expressed explicitly by Eq. (16) and can be evaluated by numerical integration. The corresponding PDF is simply the derivative with respect to $z$ of $F_{\mathrm{SNR}^{-1}}(z)$:

$$f_{\mathrm{SNR}^{-1}}(z) = \frac{d}{dz}F_{\mathrm{SNR}^{-1}}(z) = \frac{p_s \cdot p_{n,N+1} \cdot \eta}{(p_s \cdot z - p_{n,1})^2} \int_{f_1(p_s \cdot z)}^{g_1(p_s \cdot z)} dy_2 \frac{y_2}{(y_2 - p_{n,2})^2} \cdots$$
$$\cdots \int_{f_{k-1}(y_{k-1})}^{g_{k-1}(y_{k-1})} dy_k \frac{y_k}{(y_k - p_{n,k})^2} \cdots \int_{f_{N-1}(y_{N-1})}^{g_{N-1}(y_{N-1})} dy_N \frac{y_N}{(y_N - p_{n,N})^2}; \tag{25}$$

$$z \in \left[\mathrm{SNR}_{min}^{-1}; \mathrm{SNR}_{max}^{-1}\right].$$

Finally, given a random variable $G$, which is the inverse of a random variable $H$ so that $G = \frac{1}{H}$, the PDF of $G$ is computed as:

$$f_G(g) = \frac{1}{g^2} \cdot f_H\left(\frac{1}{g}\right); \tag{26}$$

where $f_H(h)$ is the PDF of the random variable $H$. Applying Eq. (26) to Eq. (25) leads to the final PDF of the SNR in presence of $N$ PDL elements on the considered optical link, which follows:

$$f_{\mathrm{SNR}}(t) = \frac{p_s \cdot p_{n,N+1} \cdot \eta}{(p_s - t \cdot p_{n,1})^2} \int_{f_1(p_s/t)}^{g_1(p_s/t)} dy_2 \frac{y_2}{(y_2 - p_{n,2})^2} \cdots \int_{f_{N-1}(y_{N-1})}^{g_{N-1}(y_{N-1})} dy_N \frac{y_N}{(y_N - p_{n,N})^2};$$
$$t \in [\mathrm{SNR}_{min}; \mathrm{SNR}_{max}]; \tag{27}$$

where the values of $\mathrm{SNR}_{min}$ and $\mathrm{SNR}_{max}$ are simply the inverse of $\mathrm{SNR}_{min}^{-1}$ and $\mathrm{SNR}_{max}^{-1}$ provided in Eq. (17). In the case of few PDL elements, it is possible to express Eq. (27) in closed form. We provide the expression for a single PDL element and for 2 PDL elements:

$$\begin{aligned} N = 1: \quad & f_{\mathrm{SNR}}(t) = \frac{p_s \cdot p_{n,N+1} \cdot \eta}{(p_s - t \cdot p_{n,1})^2}; \quad t \in [\mathrm{SNR}_{min}; \mathrm{SNR}_{max}]; \\ N = 2: \quad & f_{\mathrm{SNR}}(t) = \frac{p_s \cdot p_{n,N+1} \cdot \eta}{(p_s - t \cdot p_{n,1})^2} \cdot u(t); \end{aligned} \tag{28}$$

$$u(t) = \begin{cases} \log\left|\frac{t p_{n,3}\xi_1\xi_2}{p_s - t(p_{n,1} + p_{n,2}\xi_1)}\right| + \frac{p_{n,2}}{p_{n,3}\xi_2} \cdot \frac{t(p_{n,1} + p_{n,2}\xi_1 + p_{n,3}\xi_1\xi_2) - p_s}{p_s - t(p_{n,1} + p_{n,2}\xi_1)}; & t < \frac{p_s}{C_2} \wedge t < \frac{p_s}{D_2} \\ \log\left|\frac{\xi_1^2[p_s - t(p_{n,1} + p_{n,2}\xi_1^{-1})]}{p_s - t(p_{n,1} + p_{n,2}\xi_1)}\right| + \frac{t p_{n,2}(\xi_1^2 - 1)(p_s - t p_{n,1})}{\xi_1[p_s - t(p_{n,1} + p_{n,2}\xi_1)][p_s - t(p_{n,1} + p_{n,2}\xi_1^{-1})]} & t < \frac{p_s}{C_2} \wedge t \geq \frac{p_s}{D_2} \\ \log\left(\xi_2^2\right) + \frac{p_{n,2}}{p_{n,3}} \cdot \frac{\xi_2^2 - 1}{\xi_2} & t \geq \frac{p_s}{C_2} \wedge t < \frac{p_s}{D_2} \\ \log\left|\frac{p_s - t(p_{n,1} + p_{n,2}\xi_1^{-1})}{t p_{n,3}\xi_1^{-1}\xi_2^{-1}}\right| + \frac{p_{n,2}}{p_{n,3}\xi_2^{-1}} \cdot \frac{p_s - t(p_{n,1} + p_{n,2}\xi_1^{-1} + p_{n,3}\xi_1^{-1}\xi_2^{-1})}{p_s - t(p_{n,1} + p_{n,2}\xi_1^{-1})} & t \geq \frac{p_s}{C_2} \wedge t \geq \frac{p_s}{D_2} \end{cases}; \tag{29}$$

$$t \in [\mathrm{SNR}_{min}; \mathrm{SNR}_{max}].$$

## 3. Validation

In this section, we validate the analytical result of the previous section by means of numerical simulation. To simulate the PDL-impaired system in Fig. 1, we exploited the Monte Carlo simulator experimentally validated in [27] and enhanced in [26]. The aim of the Monte Carlo validation is to assess the accuracy of the analytical PDF under the assumptions of the proposed model, namely additive ASE noise and ideal equalization. A more detailed physical-layer validation including span-by-span amplifier gain, noise figure, and explicit nonlinear interference accumulation is left for future work. We performed $10^5$ link realizations, considering arbitrary PDL effect along the line, focusing on two scenarios. In the first, which we call "low PDL regime", the amount of PDL introduced by each device is less than 1 dB, which replicates a realistic use-case, as it was observed in many experiments [24–27]. In the second, which we call

Optics EXPRESS

"high PDL regime", the per-device PDL value is greater than 1 dB, simulating an extreme case with very high PDL deployed in the optical link. The chosen PDL values for each device are listed in Table 1. When simulating, we consider an increasing number of PDL devices in both scenarios. We start by simulating a link with just device number 1, and repeat the simulation adding devices up to the final case with all the 8 PDL devices. The noise is distributed so that each noise source injects the same noise power, and the total SNR in absence of PDL, namely the signal power over the sum of all the power of the noise sources, is equal to 15 dB.

**Table 1. PDL value for each PDL element considered for the validation**

| el. # | | 1 | 2 | 3 | 4 | 5 | 6 | 7 | 8 |
|---|---|---|---|---|---|---|---|---|---|
| PDL [dB] | low PDL | 0.3 | 0.4 | 0.7 | 0.5 | 0.6 | 0.3 | 0.8 | 0.4 |
| | high PDL | 2 | 2.1 | 1.5 | 3 | 2.5 | 1 | 2 | 1.8 |

Figures 3 and 4 show the comparison between the numerically obtained PDF of the PDL-induced SNR and the analytical expression given by Eq. (27). The PDF is plotted with respect to the SNR in linear scale, according to the derivation performed in the previous section. There is excellent agreement between theory and simulation in both the low and high PDL regimes.

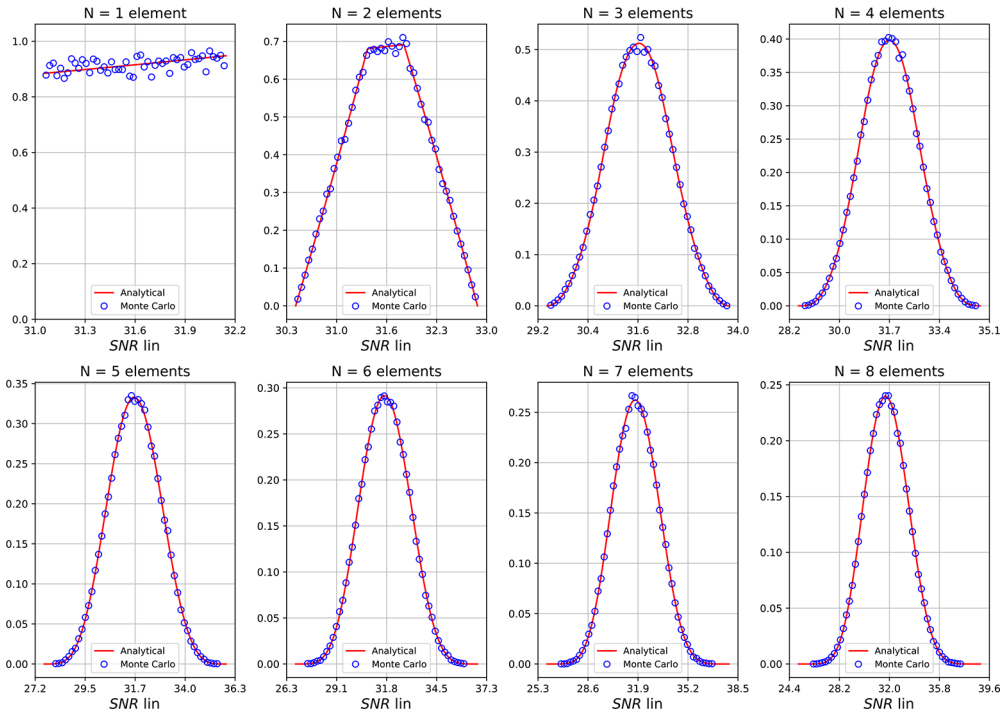


**Fig. 3.** PDL-induced SNR distribution for low-PDL regime.

The first observation is that the higher the number of PDL devices, the wider the distribution. Focusing on the low PDL regime described by Fig. 3, the distribution spans approximately from an SNR value of 31 to an SNR of 32.2 in the case of a single element. In the case of 8 elements, the extremes of the SNR are approximately 24.4 and 39.6. As expected, the PDF enlargement is even more drastic in the high PDL regime, where the SNR bounds are 7.5 and 70.7 in the case of 8 elements. This effect is in line with previous results, where the standard deviation of the distribution has been found to increase with the number of PDL devices, if the link is

Optics EXPRESS

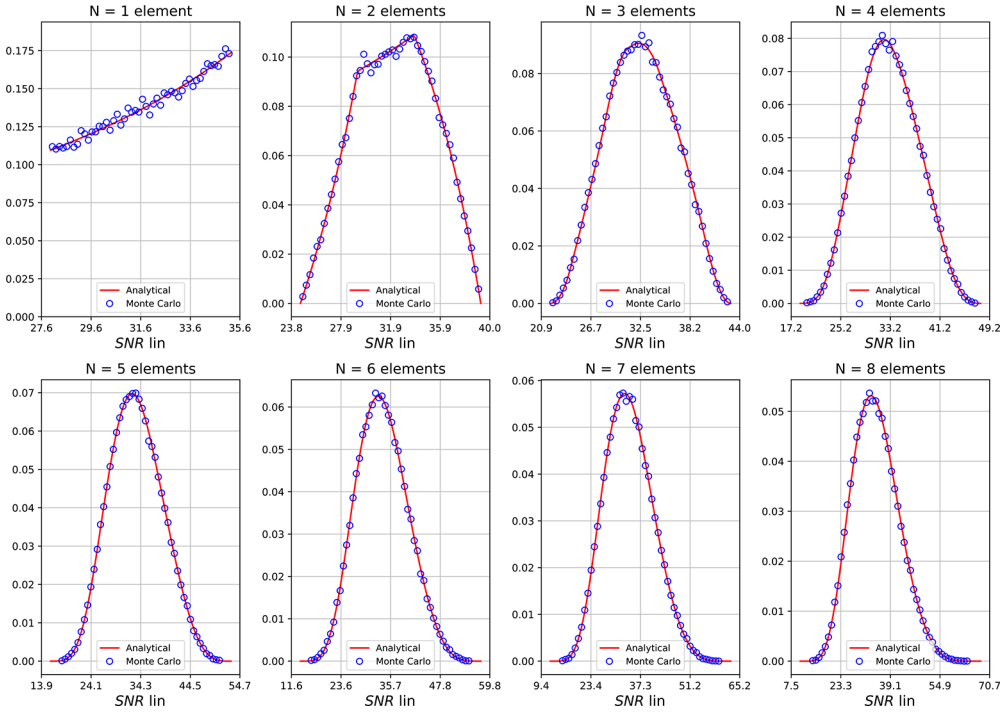


**Fig. 4.** PDL-induced SNR distribution for high-PDL regime.

composed by less than 10 devices [26,43]. A second consideration can be made about the shape of the distribution. With less than 3 PDL elements, the PDF appears to be irregular in both high and low PDL regimes. After 3 PDL elements, the shape starts to be similar to a bell. The bell symmetry is almost perfect in the case of low PDL regime, while in high PDL regime the distribution is clearly asymmetric. This justifies the assumption of Gaussianity in the case of low PDL [31]. Further works can focus on the derivation of a Gaussian approximation based on the central limit theorem, starting from the expression of $\mathrm{SNR}^{-1}$ in Eq. (4). A final observation on the computational complexity is useful for practical software implementation of Eq. (27). The mathematical problem solved in the previous sections inherits the exponential complexity already described in [38]. The exponent grows with the number of PDL devices $N$, and this can be deduced from the recursive structure of Eq. (27), which has been discussed in the derivation. With efficient coding and hardware exploitation, the evaluation of the PDF of the PDL-induced SNR with up to $N = 8$ elements, which is provided in this section, was almost instantaneous, but becomes inefficient for large values of $N$. In practical cases of optical links including many PDL devices, such as Metro Networks, the expected number of cascaded ROADMs crossed in a lightpath ranges between 3 and 8, for which the evaluation of the proposed PDF formula is fast and efficient, allowing its implementation in the transmission model of an ONDT to perform statistical margin assessment.

## 4. Conclusion

In this work, we presented the first complete analytical derivation of the probability density function of the SNR in coherent optical transmission systems impaired by polarization dependent loss (PDL). Building upon the hinge model framework for PDL statistics, we transformed the cascade of PDL elements and distributed noise sources into a tractable formulation for the SNR

Optics EXPRESS

distribution, ultimately obtaining an analytical expression for the PDF through recursive variable transformations. The resulting model captures the full statistical behavior of the PDL-induced SNR fluctuations, bridging the gap between component level attenuation randomness and its system-level quality of transmission impact.

The analytical results were validated through extensive Monte Carlo simulations across a range of realistic and extreme PDL deployment scenarios. The excellent agreement between theory and simulation confirms the accuracy of the derived PDF and highlights its ability to reproduce both the widening of the SNR distribution with increasing PDL elements and the evolution of its shape; from irregular in short links to nearly Gaussian in low PDL cases with more than three elements. These findings provide a rigorous foundation for statistical margin strategies, enabling more efficient and less conservative QoT assessment compared to worst case design rules. The model is computationally efficient for practical link configurations, such as metro networks with up to eight cascaded PDL elements. This makes the proposed formulation suitable for integration into optical network digital twins and real time physical layer estimation engines, where accurate SNR statistics are essential for adaptive margin management, rate optimization, and impairment-aware resource allocation.

The present formulation should be interpreted as an exact analytical characterization of the PDL-induced SNR statistics under the adopted assumptions, rather than as a complete end-to-end model of a practical coherent receiver. In particular, the model includes additive ASE noise and ideal equalization, while PMD, filtering-induced distortions, and practical equalizer implementation penalties are outside its scope.

Future research may extend this framework by exploring Gaussian approximations based on central limit theorem arguments, incorporating nonlinear interference contributions in greater detail, considering more general channel models that account for PMD, filtering-induced distortions, and practical equalizer effects, and leveraging the analytical PDF within machine-learning-driven control systems. A natural extension of this work is the derivation of the joint distribution of the SNRs on the two orthogonal recovered polarizations, in order to explicitly capture the complementarity induced by PDL and relate the present marginal formulation to dual-polarization QoT metrics. Overall, the proposed model offers a significant step toward enabling truly elastic, low margin, and performance predictive optical networks.

**Disclosures.** The authors declare no conflicts of interest.

**Data availability.** Data underlying the results presented in this paper are not publicly available at this time but may be obtained from the authors upon reasonable request.

## References

1. M. Filer, J. Gaudette, Y. Yin, *et al.*, "Low-margin optical networking at cloud scale [invited]," J. Opt. Commun. Netw. **11**(10), C94–C108 (2019).
2. E. Agrell, M. Karlsson, F. Poletti, *et al.*, "Roadmap on optical communications," J. Opt. **26**(9), 093001 (2024).
3. I. Tomkos, S. Azodolmolky, J. Solé-Pareta, *et al.*, "A tutorial on the flexible optical networking paradigm: State of the art, trends, and research challenges," Proc. IEEE **102**(9), 1317–1337 (2014).
4. K. Roberts, Q. Zhuge, I. Monga, *et al.*, "Beyond 100 gb/s: Capacity, flexibility, and network optimization," J. Opt. Commun. Netw. **9**(4), C12–C24 (2017).
5. D. M. Marom, Y. Miyamoto, D. T. Neilson, *et al.*, "Optical switching in future fiber-optic networks utilizing spectral and spatial degrees of freedom," Proc. IEEE **110**(11), 1835–1852 (2022).
6. M. Imran, P. M. Anandarajah, A. Kaszubowska-Anandarajah, *et al.*, "A survey of optical carrier generation techniques for terabit capacity elastic optical networks," IEEE Commun. Surv. Tutorials **20**(1), 211–263 (2018).
7. J. Müller, G. D. Rosa, O. Jovanovic, *et al.*, "Physical-layer-aware multi-band optical network planning framework for rate-adaptive transceivers," J. Opt. Commun. Netw. **16**(5), B71–B80 (2024).
8. J. Zhang, R. Vilalta, X. Yu, *et al.*, *Optical Network Virtualization* (Springer International Publishing, 2020), pp. 583–607.
9. R. Casellas, A. Giorgetti, R. Morro, *et al.*, "Virtualization of disaggregated optical networks with open data models in support of network slicing," J. Opt. Commun. Netw. **12**(2), A144–A154 (2020).
10. J. Kani, "Disaggregation and virtualization for future access and metro networks," in *Optical Fiber Communication Conference* (Optica Publishing Group, 2024), paper Tu3I.2.

Optics EXPRESS


11. A. Lord, S. J. Savory, M. Tornatore, *et al.*, "Flexible technologies to increase optical network capacity," Proc. IEEE **110**(11), 1714–1724 (2022).
12. Y. Pointurier, "Design of low-margin optical networks," J. Opt. Commun. Netw. **9**(1), A9–A17 (2017).
13. O. Karandin, A. Ferrari, F. Musumeci, *et al.*, "Probabilistic low-margin optical-network design with multiple physical-layer parameter uncertainties," J. Opt. Commun. Netw. **15**(7), C129–C137 (2023).
14. H. Nishizawa, T. Mano, K. Anazawa, *et al.*, "Optical network digital twin – commercialization barriers, value proposition, early use cases, and challenges," arXiv (2025).
15. V. Curri, "Gnpy model of the physical layer for open and disaggregated optical networking," J. Opt. Commun. Netw. **14**(6), C92–C104 (2022).
16. Q. Zhuge, X. Liu, Y. Zhang, *et al.*, "Building a digital twin for intelligent optical networks," J. Opt. Commun. Netw. **15**(8), C242–C262 (2023).
17. D. Wang, Y. Song, Y. Zhang, *et al.*, "Digital twin of optical networks: A review of recent advances and future trends," J. Lightwave Technol. **42**(12), 4233–4259 (2024).
18. I. Kaminow, "Polarization in optical fibers," IEEE J. Quantum Electron. **17**(1), 15–22 (1981).
19. F. Bruyere and O. Audouin, "Penalties in long-haul optical amplifier systems due to polarization dependent loss and gain," IEEE Photonics Technol. Lett. **6**(5), 654–656 (1994).
20. Q. Wang, G. Rajan, P. Wang, *et al.*, "Polarization dependence of bend loss for a standard singlemode fiber," Opt. Express **15**(8), 4909–4920 (2007).
21. T. A. Strasser and J. L. Wagener, "Wavelength-selective switches for roadm applications," IEEE J. Sel. Top. Quantum Electron. **16**(5), 1150–1157 (2010).
22. G. Nicholson and D. Temple, "Polarization fluctuation measurements on installed single-mode optical fiber cables," J. Lightwave Technol. **7**(8), 1197–1200 (1989).
23. A. Galtarossa, L. Palmieri, M. Schiano, *et al.*, "Statistical characterization of fiber random birefringence," Opt. Lett. **25**(18), 1322–1324 (2000).
24. A. D'Amico, G. Borraccini, S. Straullu, *et al.*, "Statistical analysis of pdl penalty on coherent transmission technologies based on wss experimental characterization," *Asia Communications and Photonics Conference* (2022), pp. 874–877.
25. G. Borraccini, A. D'Amico, S. Straullu, *et al.*, "On the characterization of pdl distribution in wavelength selective switches," *Photonics Conference* (IEEE, 2023), pp. 1–2.
26. E. Miotto, A. D'Amico, R. Ambrosone, *et al.*, "Statistical assessment of system margin in metro networks impaired by pdl," *Optical Fiber Communications Conference and Exhibition* (2025), pp. 1–3.
27. A. D'Amico, G. Borraccini, S. Straullu, *et al.*, "Experimental probing and modeling of the pdl impact on the optical signal-to-noise ratio," in *Optical Fiber Communication Conference* (Optica Publishing Group, 2023), paper W1E.6.
28. B. Huttner, C. Geiser, and N. Gisin, "Polarization-induced distortions in optical fiber networks with polarization-mode dispersion and polarization-dependent losses," IEEE J. Sel. Top. Quantum Electron. **6**(2), 317–329 (2000).
29. L. E. Nelson, C. Antonelli, A. Mecozzi, *et al.*, "Statistics of polarization dependent loss in an installed long-haul wdm system," Opt. Express **19**(7), 6790–6796 (2011).
30. OpenROADM, "Optical Specifications," April 22, 2025 Release v8.0.1, https://github.com/OpenROADM/OpenROADM_MSA_Public.
31. M. Shtaif, "Performance degradation in coherent polarization multiplexed systems as a result of polarization dependent loss," Opt. Express **16**(18), 13918–13932 (2008).
32. A. Rosso, E. Miotto, E. Virgillito, *et al.*, "Is the Gaussian channel model suitable for converged metro-access optical networks?" *25th Anniversary International Conference on Transparent Optical Networks* (2025), pp. 1–4.
33. A. Dumenil, E. Awwad, and C. Measson, "Rate optimization using so(4) transforms for pdl mitigation," in *45th European Conference on Optical Communication* (2019).
34. A. Dumenil, E. Awwad, and C. Méasson, "Pdl in optical links: A model analysis and a demonstration of a pdl-resilient modulation," J. Lightwave Technol. **38**(18), 5017–5025 (2020).
35. C. Delezoide, H. Akbari, P. Ramantanis, *et al.*, "On the detection, modeling, and mitigation of anomalous qot fluctuations in optical networks," J. Opt. Commun. Netw. **16**(5), B35–B44 (2024).
36. A. Mecozzi and M. Shtaif, "The statistics of polarization-dependent loss in optical communication systems," IEEE Photonics Technol. Lett. **14**(3), 313–315 (2002).
37. A. Galtarossa and L. Palmieri, "The exact statistics of polarization-dependent loss in fiber-optic links," IEEE Photonics Technol. Lett. **15**(1), 57–59 (2003).
38. S. Zarkosvky and M. Shtaif, "Statistical distribution of polarization-dependent loss in systems characterized by the hinge model," Opt. Lett. **45**(5), 1224–1227 (2020).
39. X. Lin and Z. Jiang, "Generalized probability density function of polarization-dependent loss in optical links," IEEE Photonics Technol. Lett. **36**(2), 79–82 (2024).
40. A. Mecozzi and M. Shtaif, "Signal-to-noise-ratio degradation caused by polarization-dependent loss and the effect of dynamic gain equalization," J. Lightwave Technol. **22**(8), 1856–1871 (2004).
41. C. Antonelli and A. Mecozzi, "Theoretical characterization and system impact of the hinge model of pmd," J. Lightwave Technol. **24**(11), 4064–4074 (2006).
42. C. Antonelli and A. Mecozzi, "Statistics of the dgd in pmd emulators," IEEE Photonics Technol. Lett. **16**(8), 1840–1842 (2004).

Optics EXPRESS


43. A. D'Amico, G. Borraccini, S. Straullu, *et al.*, "Disaggregated statistical characterization of the pdl impairment on the optical signal-to-noise ratio," *International Conference on Photonics in Switching and Computing* (2023), pp. 1–3.
44. P. Poggiolini, G. Bosco, A. Carena, *et al.*, "The gn-model of fiber non-linear propagation and its applications," J. Lightwave Technol. **32**(4), 694–721 (2014).
45. R. Dar, M. Feder, A. Mecozzi, *et al.*, "Accumulation of nonlinear interference noise in fiber-optic systems," Opt. Express **22**(12), 14199–14211 (2014).
46. N. Rossi, P. Serena, and A. Bononi, "Polarization-dependent loss impact on coherent optical systems in presence of fiber nonlinearity," IEEE Photonics Technol. Lett. **26**(4), 334–337 (2014).
47. N. Rossi, S. Musetti, P. Ramantanis, *et al.*, "The impact of kerr nonlinearity on the snr variability induced by polarization-dependent loss," J. Lightwave Technol. **37**(19), 5048–5055 (2019).
48. P. Serena, S. Musetti, S. Almonacil, *et al.*, "The Gaussian noise model extended to polarization dependent loss and its application to outage probability estimation," *European Conference on Optical Communication* (2018), pp. 1–3.
49. R. C. Jones, "A new calculus for the treatment of optical systemsi. description and discussion of the calculus," J. Opt. Soc. Am. **31**(7), 488–493 (1941).